Manuscript submitted to
AIMS' Journals
Volume **X**, Number **0X**, XX **200X**

doi:10.3934/xx.xx.xx.xx

pp. **X–XX**

STUART-TYPE POLAR VORTICES ON A ROTATING SPHERE

Adrian Constantin*

Faculty of Mathematics, University of Vienna
Oskar-Morgenstern-Platz 1
1090 Vienna, Austria

Darren G. Crowdy

Department of Mathematics, Imperial College London
180 Queen's Gate
London SW7 2AZ, United Kingdom

Vikas S. Krishnamurthy

Faculty of Mathematics, University of Vienna
Oskar-Morgenstern-Platz 1
1090 Vienna, Austria

Miles H. Wheeler

Department of Mathematical Sciences, University of Bath
Bath BA2 7AY, United Kingdom

(Communicated by the associate editor name)

Abstract. Stuart vortices are among the few known smooth explicit solutions of the planar Euler equations with a nonlinear vorticity, and they can be adapted to model inviscid flow on the surface of a fixed sphere. By means of a perturbative approach we show that the method used to investigate Stuart vortices on a fixed sphere provides insight into the dynamics of the large-scale zonal flows on a rotating sphere that model the background flow of polar vortices. Our approach takes advantage of the fact that while a sphere is spinning around its polar axis, every point on the sphere has the same angular velocity but its tangential velocity is proportional to the distance from the polar axis of rotation, so that points move fastest at the Equator and slower as we go towards the poles, both of which remain fixed.

1. **Introduction.** A polar vortex is a persistent prograde planetary-scale atmospheric flow that encircles the pole of a rotating planetary body in high latitudes. Distinct polar vortices have been observed on Earth, Mars, Venus, Saturn, Titan, Jupiter, Neptune and Uranus [16]. Of the extraterrestrial polar vortices, the most comprehensive observations are available for Saturn, where these flows are remarkably steady; see the data in [9]. While Venus and Mars are closer to Earth, their polar vortices have a more transient character [19].

There are numerous observational and modelling studies to gain insight into the structure and dynamics of polar vortices. The first step is the quest for simplifying assumptions supported by observational evidence. This is achieved by evaluating non-dimensional parameters that arise in connection with specific physical effects, omitting from the model physical factors if the associated parameter is small. Since

This research was supported by the WWTF research grant MA16-009.

* Corresponding author: Adrian Constantin.

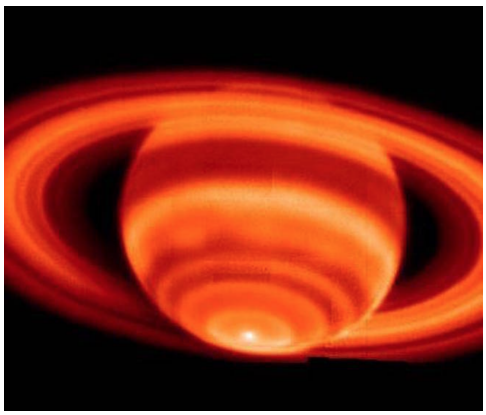

FIGURE 1. Image showing the hot spot centered on Saturn's South Pole (the core of the southern polar vortex, at the bottom of the image), taken from the observatory in Hawaii with infrared radiation sensitive to temperatures in Saturn's upper troposphere [Image credit: NASA/JPL-CalTech/Space Science Institute]. A similar hot spot is found at Saturn's North Pole.

in a polar vortex the ratio of vertical speed to horizontal speed is typically smaller than 10^{-4} [17], we can neglect the vertical component of the velocity and thus study a 2D zonal flow model. Furthermore, due to the large length-scales in a polar vortex, the Reynolds number $\mathfrak{Re}$ and the Ekman number $\mathcal{E}$ are typically very large and very small, respectively, e.g. $\mathfrak{Re} > 10^{12}$ and $\mathcal{E} < 10^{-14}$ for Saturn [1]. Therefore the assumption of an inviscid flow with leading-order Coriolis effects is geophysically reasonable. Regarding the density variations of atmospheric flows, the appropriate setting is that of a density that varies with height [22]. Finally, the fact that there are many parameters (e.g. size of the planet, distance from the Sun) that make planetary atmospheres difficult to compare, the vertical component of relative vorticity, evaluated on an isentropic surface (a level set of the potential temperature), is the main characteristic used in case studies [16]. Throughout this paper we restrict ourselves to an isothermal atmospheric flow. For example, Titan's atmosphere above 500 km altitude is essentially isothermal at about 170°K [4]. Also, during the ten-year span of the Cassini mission, the upper troposphere temperatures in both of Saturn's hot spots (the cores of its two polar vortices, see Figure 1) were nearly uniform at about 90°K, despite seasonal shifts in temperature in their vicinity, latitude-wise but also in the stratosphere above; see [2].

In Section 2 we will show that the two-dimensional, stratified, steady flow in a polar vortex is modeled in spherical geometry by the *vorticity equation*

$$\nabla^2_\Sigma \psi - 2\omega \cos\theta = F(\psi) \tag{1}$$

for the stream function $\psi(\theta, \phi)$. Here ∇^2_Σ is the Laplace-Beltrami operator on the unit sphere, θ is the polar angle, ϕ is the azimuthal angle, ω is the inverse Rossby number based on the rotation rate of the planet. The vorticity due to the rotation of the planet—the planetary vorticity—is given by the term $2\omega\cos\theta$, and F is the relative vorticity function specific to the flow. Equation (1) was derived as a model for ocean gyres on Earth in [5], utilizing a shallow-water approximation and assuming that density variations in the fluid are absent.

The vorticity equation (1) represents the counterpart in spherical coordinates of the mid-latitude β-plane model due to Fofonoff [11][1], in which the Laplace-Beltrami operator is replaced by a planar Laplacian operator and the background vorticity term $2\omega\cos\theta$ in replaced by its first-order Taylor expansion about a fixed co-latitude θ_0. At the North and South poles ($\theta_0 = 0$ and $\theta_0 = \pi$), the first-order term vanishes, and in the research literature a second-order γ-plane approximation is typically used instead of the β-plane approximation in polar regions (see [26]). For these approximations to be consistent, however, the Laplace-Beltrami operator should also be expanded to higher order. Unfortunately, the resulting operators have less structure than either the Laplace-Beltrami operator or the planar Laplacian and are hence difficult to work with. For linear functions $F(\psi)$ closed-form explicit solutions of Fofonoff's equation may be found in terms of eigenfunctions of the planar Laplace operator with a Dirichlet boundary condition [11]. Analogously, explicit solutions to (1) for linear functions $F(\psi)$ are provided by the eigenfunctions of the Laplace-Beltrami operator on the sphere [15, 13, 25]. These Rossby waves and Rossby–Haurwitz waves were generalised using piecewise linear functions $F(\psi)$, for instance by Wu and Verkley [27]. While the spherical harmonics solutions have finitely many degrees of freedom, the family of solutions that we construct is richer while arguably having a simpler form. The steady background state studied here can be perturbed by Rossby waves, but this will be pursued elsewhere.

Since the relative vorticity typically presents strong variations close to the core of the polar vortex (see the data in [3]), it is poorly approximated by linear functions. This motivates the search for nonlinear functions $F(\psi)$ that could accommodate either explicit solutions of the vorticity equation (1), or solutions of (1) whose deviation from a closed-form expression can be estimated with accuracy. The celebrated Stuart vortices [23] in planar flows are closed-form solutions of the planar vorticity equation in the absence of background rotation i.e. when $\omega = 0$. The vorticity function for Stuart vortices is exponential: $F(\psi) = a\,\mathrm{e}^{b\psi}$, where a and b are real constants. Stuart vortex solutions were generalized to the surface of a stationary sphere using stereographic projection techniques from complex analysis by Crowdy [8]. Stuart vortices on a stationary sphere are solutions to (1) when $\omega = 0$, and the vorticity function takes the form $F(\psi) = a\,\mathrm{e}^{b\psi} + c$, where c is a real constant.

We investigate here a class of vortex solutions for shallow-water flows on a rotating sphere, which we call 'Stuart-type' vortices. These are the counterparts on a rotating sphere of Stuart vortices on a stationary sphere [8], and also have the vorticity function $F(\psi) = a\,\mathrm{e}^{b\psi} + c$. We show that they represent the leading order solution in a shallow-water limit, and obtain rigorous error bounds on their deviation from the stationary sphere Stuart solution. We do so by means of an interplay between the geometric features encoded in the stereographic projection and the comparison method for nonlinear elliptic partial differential equations. The provided sharp estimates permit us to visualize the streamline-pattern of the flow. At mid-latitudes a related approach was used in [6] to obtain error bounds in the context of ocean gyres. For polar regions, the approach used here is more accurate.

This paper is organized as follows. Starting from the governing Euler equation and the conservation of mass, we derive the vorticity equation for the horizontal flow in rotating spherical coordinates by means of the shallow-water approximation in Section 2. We discuss Stuart vortices on a sphere in Section 3, and their relevance to polar vortices in Section 4, with special attention devoted to Saturn's polar vortices.

[1]See [24] for a description using modern notation.

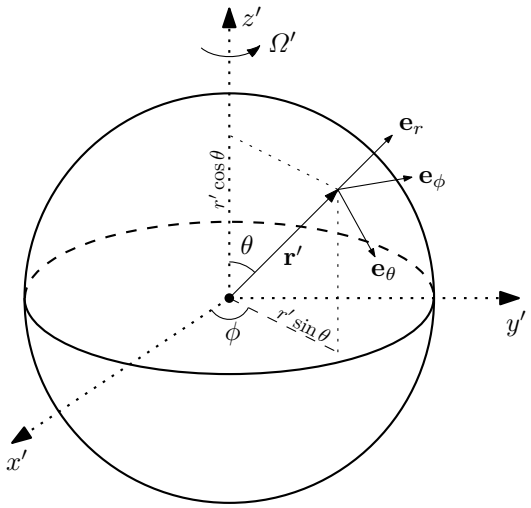

FIGURE 2. The spherical coordinate system describing flow on a rotating planet. The coordinate system is fixed with respect to the planet rotating with an angular speed Ω' about the z' axis of the Cartesian coordinate system (x', y', z'). The spherical coordinates are (r', θ, ϕ) where $r' = |\mathbf{r}'|$ is the distance from the origin at the planet's center, θ is the polar angle (co-latitude) and ϕ is the angle of longitude. The North Pole of the planet is at $\theta = 0$ and the South Pole is at $\theta = \pi$.

In Section 5 we present an example of flow visualisation, representing the streamline pattern for an approximate solution of the type discussed in Section 4. Finally, in Section 6 we overview the material presented throughout the paper.

2. Governing equations.

We consider the right-handed spherical coordinate system (r', θ, ϕ) shown in Figure 2. Here r' is the distance from the center of the sphere, $0 \le \theta \le \pi$ is the polar angle (so $\pi/2 - \theta$ is the latitude), and $0 \le \phi < 2\pi$ is the azimuthal angle (longitude). Primes denote physical, dimensional variables while dimensionless quantities are denoted by unprimed variables. The unit vectors in this coordinate system are $(\mathbf{e}_r, \mathbf{e}_\theta, \mathbf{e}_\phi)$; $\mathbf{e}_\phi$ points from West to East and $\mathbf{e}_\theta$ from North to South. The corresponding velocity components are (w', v', u') and their evolution for inviscid flow is governed by the components of the Euler equation (see [12])

$$\frac{\mathrm{D}w'}{\mathrm{D}t'} - \frac{u'^2 + v'^2}{r'} - 2\Omega' u' \sin\theta - \Omega'^2 r' \sin^2\theta = -\frac{1}{\rho'}\frac{\partial p'}{\partial r'} - g', \tag{2a}$$

$$\frac{\mathrm{D}v'}{\mathrm{D}t'} + \frac{v'w' - u'^2\cot\theta}{r'} - 2\Omega' u' \cos\theta - \Omega'^2 r' \sin\theta\cos\theta = -\frac{1}{\rho'}\frac{1}{r'}\frac{\partial p'}{\partial \theta}, \tag{2b}$$

$$\frac{\mathrm{D}u'}{\mathrm{D}t'} + \frac{u'v'\cot\theta + u'w'}{r'} + 2\Omega'(v'\cos\theta + w'\sin\theta) = -\frac{1}{\rho'}\frac{1}{r'\sin\theta}\frac{\partial p'}{\partial \phi}, \tag{2c}$$

where the material derivative $\mathrm{D}/\mathrm{D}t'$ in spherical coordinates is given by the expression

$$\frac{\mathrm{D}}{\mathrm{D}t'} = \frac{\partial}{\partial t'} + \frac{u'}{r'\sin\theta}\frac{\partial}{\partial\phi} + \frac{v'}{r'}\frac{\partial}{\partial\theta} + w'\frac{\partial}{\partial r'}. \tag{3}$$

Here p' and ρ' are the pressure and density in the fluid, Ω' is the constant rate of rotation of the planet and g' is the acceleration due to gravity, taken to be a constant. The conservation of mass in spherical coordinates takes the form

$$\frac{\mathrm{D}\rho'}{\mathrm{D}t'} + \rho'\left(\frac{1}{r'\sin\theta}\frac{\partial u'}{\partial\phi} + \frac{1}{r'\sin\theta}\frac{\partial}{\partial\theta}(v'\sin\theta) + \frac{1}{r'^2}\frac{\partial}{\partial r'}(r'^2 w')\right) = 0. \tag{4}$$

2.1. **Non-dimensionalisation and the vorticity equation.** We now non-dimensionalise the governing equations (2) and (4) using the following length and velocity scales.

$$\begin{aligned} R' &: \text{ radius of the planet} \\ H' &: \text{ mean height of the relevant atmospheric layer} \\ U' &: \text{ suitable horizontal velocity scale} \\ W' &: \text{ suitable vertical velocity scale} \\ \overline{\rho}' &: \text{ average density in the relevant atmospheric layer} \end{aligned} \tag{5}$$

The inverse Rossby number is defined as

$$\omega = \frac{\Omega' R'}{U'}, \tag{6}$$

The two small parameters describing the flow are

$$\varepsilon = \frac{H'}{R'} \quad \text{and} \quad k = \frac{W'}{U'}, \tag{7}$$

where ε is the usual shallowness parameter and k is the ratio between the vertical and horizontal velocity scales. The new dimensionless variables z, w, v, u and p are given by

$$\begin{gathered} r' = R' + H'z, \qquad w' = W'w, \qquad (v', u') = U'(v, u), \\ \rho' = \overline{\rho}'\rho, \qquad p' = \overline{\rho}' U'^2 p. \end{gathered} \tag{8}$$

In the shallow-water regime for steady flow with the scaling $k \ll \varepsilon \ll 1$, the Euler equations (2) have the following form at leading order for the tangential flow (u, v):

$$0 = \frac{\partial P}{\partial z}, \tag{9a}$$

$$\frac{u}{\sin\theta}\frac{\partial v}{\partial\phi} + v\frac{\partial v}{\partial\theta} - u^2\cot\theta - 2\omega u\cos\theta = -\frac{\partial P}{\partial\theta}, \tag{9b}$$

$$\frac{u}{\sin\theta}\frac{\partial u}{\partial\phi} + v\frac{\partial u}{\partial\theta} + uv\cot\theta + 2\omega v\cos\theta = -\frac{1}{\sin\theta}\frac{\partial P}{\partial\phi}. \tag{9c}$$

Here the density $\rho = \rho(z)$ at leading order and the dynamic pressure P is defined by

$$P = p + \frac{g'H'}{(U')^2}\int_0^z \rho(z)\,\mathrm{d}z. \tag{10}$$

The conservation of mass (4) has the leading order form

$$\frac{\partial u}{\partial\phi} + \frac{\partial}{\partial\theta}(v\sin\theta) = 0, \tag{11}$$

which guarantees the existence of a stream function, $\psi(\theta,\phi)$, satisfying

$$u = -\frac{\partial\psi}{\partial\theta} \quad \text{and} \quad v = \frac{1}{\sin\theta}\frac{\partial\psi}{\partial\phi}. \tag{12}$$

The elimination of the pressure P between the last two equations in (9) gives the vorticity equation

$$\left[\frac{\partial\psi}{\partial\phi}\frac{\partial}{\partial\theta} - \frac{\partial\psi}{\partial\theta}\frac{\partial}{\partial\phi}\right]\left(\nabla^2_\Sigma\psi - 2\omega\cos\theta\right) = 0, \tag{13}$$

in which ∇^2_Σ is the Laplace-Beltrami operator on the surface of a unit sphere, given by,

$$\nabla^2_\Sigma = \frac{\partial^2}{\partial\theta^2} + \cot\theta\frac{\partial}{\partial\theta} + \frac{1}{\sin^2\theta}\frac{\partial^2}{\partial\phi^2}. \tag{14}$$

By direct inspection any solution of (1) solves (13). Moreover, throughout regions where $(\partial\psi/\partial\theta, \partial\psi/\partial\phi) \neq (0,0)$, we see from (13) that the rank theorem (see [18]) yields (1). As pointed out in the introduction, (1) is the counterpart in spherical coordinates of Fofonoff's β-plane model. Equation (13) was derived in [5], assuming constant density, as a model for ocean gyres.

3. **Stuart vortices on a sphere.** The planetary vorticity $2\omega\cos\theta$ in (1) is set by the rotation of the planet, but the relative vorticity $F(\psi)$ is specific to the particular flow conditions. If we ignore the planetary vorticity by setting $\omega = 0$, the vorticity equation (1) describes steady vortex solutions, for flows in the plane (using the planar Laplacian in (1)) or on the surface of a stationary sphere (using the Laplace-Beltrami operator in (1)). Considerations related to Stuart vortices (see [23, 8]) offer prospects for the study of solutions to (1) for nonlinear vorticity functions of the form $F(\psi) = a\,\mathrm{e}^{b\psi} + c$ with suitable real constants a, b, and c. The interaction between the non-constant planetary vorticity term and the nonlinear relative vorticity term $F(\psi)$ in (1) considerably alters the underlying mathematical structure of the problem.

The *stereographic projection* is a one-to-one mapping of the surface of the unit sphere to the equatorial plane $z = 0$ (see [20]), as shown in Figure 3. The North pole $(0,0,1)$ is mapped to the point at infinity and the South pole $(0,0,-1)$ is mapped to the origin of coordinates. We take the Cartesian coordinates in the equatorial plane to be (X,Y) and define the complex ζ-plane, $\zeta = X + \mathrm{i}Y$. The stereographic projection yields the following useful formulas in terms of the polar angle θ and the longitude ϕ:

$$\zeta = \cot(\theta/2)\,\mathrm{e}^{\mathrm{i}\phi}, \tag{15a}$$

$$\cos\theta = \frac{\zeta\bar{\zeta}-1}{\zeta\bar{\zeta}+1} \quad \text{and} \quad \sin\theta = \frac{2\sqrt{\zeta\bar{\zeta}}}{\zeta\bar{\zeta}+1}. \tag{15b}$$

Here $\bar{\zeta}$ is the complex conjugate of ζ. In the ζ-plane we consider a formal change of variables from (X,Y) to $(\zeta,\bar{\zeta})$ and then the stream function can be considered as a function of the variables $(\zeta,\bar{\zeta})$. Equation (1) can be rewritten using the formulas (15) as

$$(\zeta\bar{\zeta}+1)^2\psi_{\zeta\bar{\zeta}} = 2\omega\,\frac{\zeta\bar{\zeta}-1}{\zeta\bar{\zeta}+1} + F(\psi), \tag{16}$$

where subscripts denote partial derivatives, $\psi_{\zeta\bar{\zeta}} = \partial^2\psi/\partial\zeta\partial\bar{\zeta}$; see [6, 8].

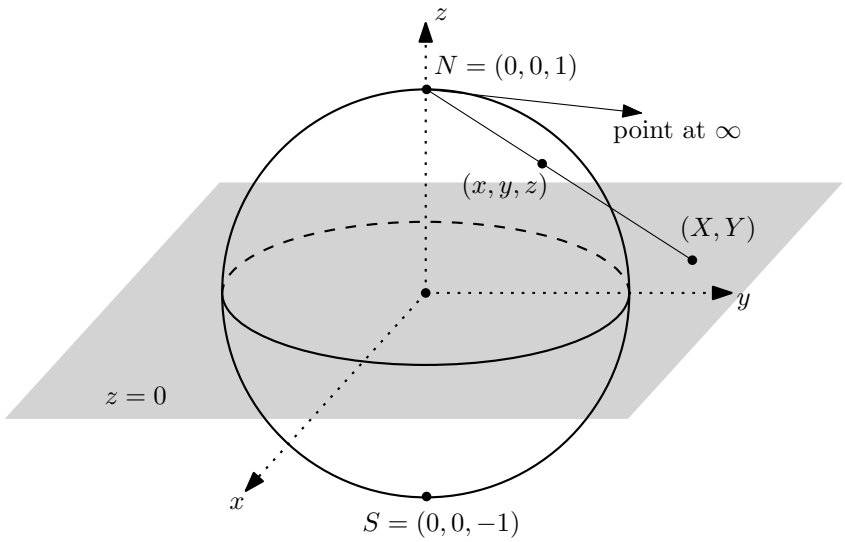

FIGURE 3. The stereographic projection maps the point (x, y, z) on the unit sphere with the North Pole N excised to the intersection point (X, Y) of the equatorial plane with the ray from N to (x, y, z). The point N itself is mapped to the point at infinity on the equatorial plane.

Solutions of (16) with $\omega = 0$ and the choice $F(\psi) = a\,\mathrm{e}^{b\psi} + c$ for suitable real constants $a \neq 0$, $b \neq 0$, and c, were obtained by Crowdy [8] by considering the following change of dependent variables, from $\psi(\zeta, \bar{\zeta})$ to $\varphi(\zeta, \bar{\zeta})$:

$$\psi(\zeta, \bar{\zeta}) = \varphi(\zeta, \bar{\zeta}) + \frac{2}{b}\,\ln(\zeta\bar{\zeta} + 1), \tag{17a}$$

$$F(\psi) = a\,\mathrm{e}^{b\psi} + c = a(\zeta\bar{\zeta} + 1)^2\,\mathrm{e}^{b\varphi} + c. \tag{17b}$$

We employ the same change of dependent variables for a rotating sphere i.e. $\omega \neq 0$. Choosing the constant $c = 2/b + 2\omega$, (16) is transformed into

$$\varphi_{\zeta\bar{\zeta}} = a\,\mathrm{e}^{b\varphi} + \frac{4\omega\zeta\bar{\zeta}}{(\zeta\bar{\zeta} + 1)^3}. \tag{18}$$

When $\omega = 0$, (18) reduces to the planar Liouville equation

$$(\varphi_0)_{\zeta\bar{\zeta}} = a\,\mathrm{e}^{b\varphi_0} \tag{19}$$

whose closed-form solution $\varphi_0(\zeta, \bar{\zeta})$ for $ab > 0$ is (see [14, 7])

$$\varphi_0(\zeta, \bar{\zeta}) = \frac{2}{b}\,\ln\left(\frac{2|f'(\zeta)|}{2 - ab|f(\zeta)|^2}\right), \tag{20}$$

where $f(\zeta)$ is an analytic function. Choosing this function provides us infinitely-many degrees of freedom as discussed in the introduction. The associated stream function is given by

$$\psi_0(\zeta, \bar{\zeta}) = \frac{2}{b}\,\ln\left(\frac{2|f'(\zeta)|(\zeta\bar{\zeta} + 1)}{2 - ab|f(\zeta)|^2}\right). \tag{21}$$

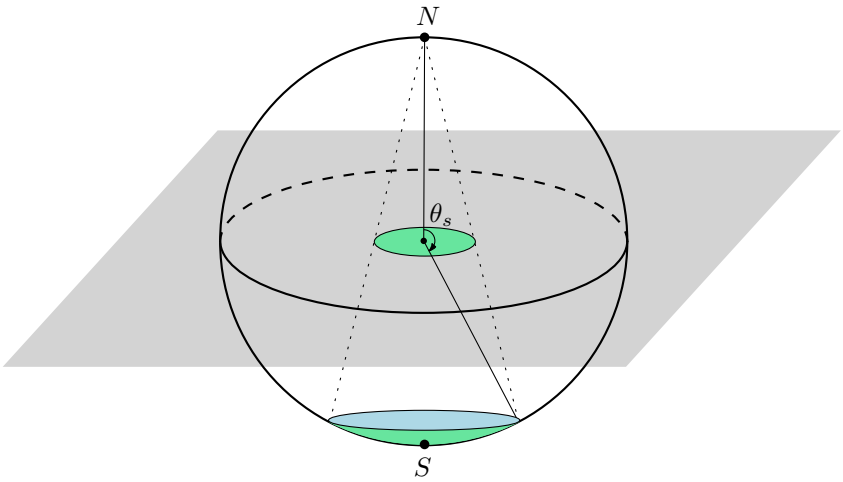

FIGURE 4. Stereographic projection of a spherical cap onto the equatorial plane. The cap near the South pole (S) encloses the vortex region and has boundary co-latitude θ_s.

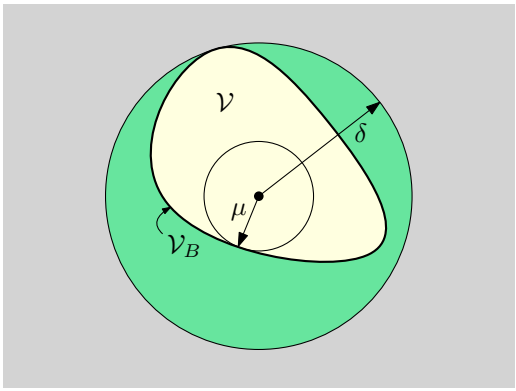

FIGURE 5. The projected vortex region $\mathcal{V}$ in the projected plane, with maximum radius δ and minimum radius μ. The boundary of $\mathcal{V}$ is denoted by $\mathcal{V}_B$.

4. **Polar vortices as approximate solutions of the Liouville equation.** We now use the explicit stream function ψ_0 given by (21) to approximate a solution ψ to (1) with the nonlinear relative vorticity

$$F(\psi) = a\,\mathrm{e}^{b\psi} + \frac{2}{b} + 2\omega, \tag{22}$$

for parameters a and b satisfying $ab > 0$. This approximation is valid near the South pole of the planet; a similar approximation works at the North pole. The error bound in the approximation is given in terms of the inverse Rossby number ω and the extent of the polar vortex, where the latter is measured in terms of the minimum co-latitude θ_s containing the vortex, as shown in Figure 4. The spherical

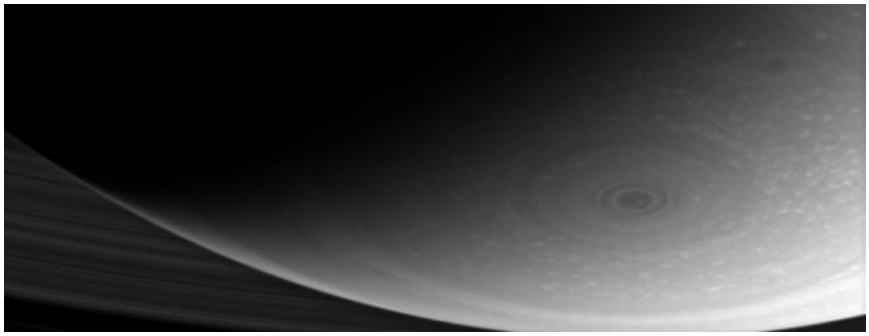

FIGURE 6. The eye of the stationary vortex centered on Saturn's South Pole and extending to 88.5°S, captured in 2008 by NASA's Cassini spacecraft using thermal radiation, is about 2000 km across and features peak prograde winds of 170 $\mathrm{m\,s^{-1}}$ [Image credit: NASA/JPL-CalTech/Space Science Institute].

cap $\theta_s \le \theta \le \pi$ is projected to the region $X^2 + Y^2 \le \delta^2$ where

$$\delta = \cot\left(\frac{\theta_s}{2}\right). \tag{23}$$

In terms of ω and δ, we obtain the pointwise error bound

$$-\omega\delta^4 \le \psi(X,Y) - \psi_0(X,Y) \le 0 \tag{24}$$

inside the vortex region.

The estimate (24) shows that if the diameter of the polar vortex region is sufficiently small, then the streamline pattern for ψ is a small perturbation of the level sets of the explicit function ψ_0 that is typically $O(\delta^2)$; see Section 5. For example, for Saturn we have $R' = 60,268$ km, $U' = 150\ \mathrm{m\,s^{-1}}$, $W' = 10^{-3}\mathrm{m\ s^{-1}}$, $\Omega' = 1.63 \times 10^{-4}\ \mathrm{s^{-1}}$, $H' = 50$ km for the upper troposphere, with the eye of the the vortex at Saturn's South Pole within 1.5° degrees of latitude from the South Pole (see the data in [9] and Figure 6); therefore we have $\varepsilon \approx 10^{-3}$, $k \approx 10^{-5}$. From (6) and (23) we estimate $\omega \approx 65$ and $\delta \approx 0.013$. Consequently, in this setting the error bound in (24) is about 2×10^{-6}.

4.1. **Error bound through sub- and super-solutions.** In this subsection we obtain the error bound (24) relying on the method of sub- and super-solutions for semilinear elliptic partial differential equations. The boundary of the steady polar vortex is a level set of the stream function, say $\psi = 0$. The exact solution ψ_0 also satisfies the condition $\psi_0 = 0$ on this boundary so that the deviation $\psi - \psi_0$ vanishes there. We solve for the deviation of the solution on the rotating sphere from the exact solution φ_0 in (20),

$$\widetilde{\varphi} = \varphi - \varphi_0 = \psi - \psi_0, \tag{25}$$

where the second equality follows from (17a).

The stereographic projection of the polar vortex is the planar region $\mathcal{V}$ shown in Figure 5. Let us denote the boundary of the projected vortex region $\mathcal{V}$ by $\mathcal{V}_B$. In terms of the Cartesian coordinates (X, Y) on the complex ζ-plane, we can write

(18) as the semilinear elliptic equation

$$\nabla^2\varphi = 4a\,\mathrm{e}^{b\varphi} + \frac{16\omega(X^2+Y^2)}{(1+X^2+Y^2)^3}, \tag{26}$$

where $\nabla^2 = \partial^2/\partial X^2 + \partial^2/\partial Y^2$ is the planar Laplace operator. Similarly (19) becomes

$$\nabla^2\varphi_0 = 4a\,\mathrm{e}^{b\varphi_0}. \tag{27}$$

Combining (26) and (27), we see that the deviation $\widetilde{\varphi}$ obeys the equation

$$\begin{cases} -\nabla^2\widetilde{\varphi} + 4a\,\mathrm{e}^{b\varphi_0}\left(\mathrm{e}^{b\widetilde{\varphi}} - 1\right) + \dfrac{16\omega(X^2+Y^2)}{(X^2+Y^2+1)^3} = 0 \quad \text{in } \mathcal{V}, \\ \qquad\qquad\qquad\qquad\qquad\qquad\qquad\qquad \widetilde{\varphi} = 0 \quad \text{on } \mathcal{V}_B. \end{cases} \tag{28}$$

To proceed, we rely on the comparison method for solutions of nonlinear elliptic partial differential *inequalities*. Consider twice continuously differentiable functions $\widetilde{\varphi}_{\mathrm{sub}}$, $\widetilde{\varphi}^{\mathrm{sup}}$ on the domain $\mathcal{V}$ together its boundary $\mathcal{V}_B$. $\widetilde{\varphi}_{\mathrm{sub}}$ is called a *sub-solution* of (28) if it satisfies

$$\begin{cases} -\nabla^2\widetilde{\varphi}_{\mathrm{sub}} + 4a\,\mathrm{e}^{b\varphi_0}\left(\mathrm{e}^{b\widetilde{\varphi}_{\mathrm{sub}}} - 1\right) + \dfrac{16\omega(X^2+Y^2)}{(X^2+Y^2+1)^3} \le 0 \quad \text{in } \mathcal{V}, \\ \qquad\qquad\qquad\qquad\qquad\qquad\qquad\qquad \widetilde{\varphi}_{\mathrm{sub}} \le 0 \quad \text{on } \mathcal{V}_B. \end{cases} \tag{29}$$

Similarly $\widetilde{\varphi}^{\mathrm{sup}}$ is called a *super-solution* of (28) if it satisfies

$$\begin{cases} -\nabla^2\widetilde{\varphi}^{\mathrm{sup}} + 4a\,\mathrm{e}^{b\varphi_0}\left(\mathrm{e}^{b\widetilde{\varphi}^{\mathrm{sup}}} - 1\right) + \dfrac{16\omega(X^2+Y^2)}{(X^2+Y^2+1)^3} \ge 0 \quad \text{in } \mathcal{V}, \\ \qquad\qquad\qquad\qquad\qquad\qquad\qquad\qquad \widetilde{\varphi}^{\mathrm{sup}} \ge 0 \quad \text{on } \mathcal{V}_B. \end{cases} \tag{30}$$

The existence of a sub-solution and a super-solution with the property $\widetilde{\varphi}_{\mathrm{sub}} \le \widetilde{\varphi}^{\mathrm{sup}}$ ensures the existence of a solution $\widetilde{\varphi}$ such that $\widetilde{\varphi}_{\mathrm{sub}} \le \widetilde{\varphi} \le \widetilde{\varphi}^{\mathrm{sup}}$ everywhere in the domain $\mathcal{V}$ [21].

It is easily verified by substituting in (30) that $\widetilde{\varphi}^{\mathrm{sup}} = 0$ is a super-solution, keeping in mind that $\omega > 0$. Substituting the expression

$$\widetilde{\varphi}_{\mathrm{sub}}(X,Y) = \omega\left((X^2+Y^2)^2 - \delta^4\right) \tag{31}$$

in (29) it can be verified that (31) is a sub-solution. To see this, note that since the region $\mathcal{V}$ is contained in the disk $X^2+Y^2 < \delta^2$, we have $\widetilde{\varphi}_{\mathrm{sub}} < 0 = \widetilde{\varphi}^{\mathrm{sup}}$ in $\mathcal{V}$. Then using (31) and after some algebra, (29) becomes

$$-(X^2+Y^2)\left[1 - \frac{1}{(X^2+Y^2+1)^3}\right] + \frac{a\,\mathrm{e}^{b\varphi_0}}{4\omega}\left(\mathrm{e}^{b\widetilde{\varphi}_{\mathrm{sub}}} - 1\right) \le 0 \tag{32}$$

It is clear that the first term is always non-positive; since $\widetilde{\varphi}_{\mathrm{sub}} < 0$, the second term is always non-positive since $ab > 0$. Thus the method of sub- and super-solutions ensures the existence of a solution $\widetilde{\varphi}$ to (28) with $\widetilde{\varphi}_{\mathrm{sub}} \le \widetilde{\varphi} \le \widetilde{\varphi}^{\mathrm{sup}}$. From (31), we have $\widetilde{\varphi}_{\mathrm{sub}} \ge -\omega\delta^4$, and therefore the desired error estimate (24) follows from (25).

4.2. **Sign and monotonicity of the relative vorticity.** The main features observed on Saturn are a relative vorticity that is positive and whose longitude-averaged values increase as we approach the core of the vortex at the South Pole (see the data in [9]). We now show that the restriction

$$|a| + \frac{2}{|b|} < 2\omega \tag{33}$$

on the relative sizes of $a < 0$ and $b < 0$ ensures that the flow induced by the stream function ψ_0 has these features. In order to take longitudinal averages of the relative vorticity, we restrict our attention to the smallest disc contained within the polar vortex region. In the stereographically projected plane, this is the disc of radius μ shown in Figure 5.

First, we show that the relative vorticity $F(\psi_0) > 0$ in this region $\zeta\bar{\zeta} < \mu^2$. Since $a < 0$ and $b < 0$, we have

$$\begin{cases} -\nabla^2\varphi_0 = 4|a|\,\mathrm{e}^{-|b|\varphi_0} > 0 & \text{in } \mathcal{V}, \\ \varphi_0 \geq \dfrac{2}{|b|}\ln(1+\mu^2) & \text{on } \mathcal{V}_B. \end{cases} \tag{34}$$

The maximum principle for superharmonic functions therefore ensures that $\varphi_0 \geq 2\ln(1+\mu^2)/|b|$ in $\mathcal{V}$ (see [10]). Combining this lower bound for φ_0 with (17a) yields

$$\begin{aligned} F(\psi_0) &= a\,\mathrm{e}^{b\varphi_0}(1+\zeta\bar{\zeta})^2 + 2\omega + \frac{2}{b} \\ &\geq -|a|\frac{(1+\zeta\bar{\zeta})^2}{(1+\mu^2)^2} + 2\omega - \frac{2}{|b|} \end{aligned} \tag{35}$$

throughout $\mathcal{V}$. Consequently, using (33) within the region $\zeta\bar{\zeta} \leq \mu^2$ yields

$$F(\psi_0) \geq 2\omega - |a| - \frac{2}{|b|} > 0. \tag{36}$$

We conclude our argument by noting that the relative vorticity $F(\psi)$ is well approximated by $F(\psi_0)$ because of the error bound (24) on $\psi - \psi_0$.

We next show that the longitude-averaged values of the relative vorticity $F(\psi_0)$ increase as we approach the core of the vortex at the South Pole. To see this, it is sufficient to check that $F(\psi_0)$ is superharmonic in this region (see [10]). Indeed, differentiating (35) and using (27), we find that $\nabla^2 F(\psi_0)$ is given by

$$\frac{a}{4}(1+X^2+Y^2)e^{b\varphi_0}(Q_1+Q_2) + a^2 b e^{2b\varphi_0}(1+X^2+Y^2)^2, \tag{37}$$

where the terms Q_1 and Q_2 are given by

$$Q_1 = b^2(1+X^2+Y^2)(\partial_X\varphi_0)^2 + 8bX(\partial_X\varphi_0) + 8\Big(\frac{1}{2} + \frac{X^2}{1+X^2+Y^2}\Big), \tag{38}$$

$$Q_2 = b^2(1+X^2+Y^2)(\partial_Y\varphi_0)^2 + 8bY(\partial_Y\varphi_0) + 8\Big(\frac{1}{2} + \frac{Y^2}{1+X^2+Y^2}\Big). \tag{39}$$

Thinking of Q_1 and Q_2 as quadratic functions of $\partial_X\varphi_0$ and $\partial_Y\varphi_0$, respectively, we can check that each of the summands in (37) is negative. Here we need that $X^2+Y^2 < 1$, but $X^2+Y^2 < \delta \ll 1$ so this is not a restriction. Thus $-\nabla^2 F(\psi_0) > 0$ so that $F(\psi_0)$ is superharmonic.

Remark. The North Pole is mapped to the point at infinity, as shown in Figure 3. Regions within a few degrees of latitude from the North Pole therefore correspond to $|\zeta| > \Delta$, for some $\Delta \gg 1$. An analysis similar to that performed in Section 4.1 yields an approximation result for the stream function of the North polar vortex. Also, considerations analogous to those above (but with $a > 0$ and $b > 0$) ensure that the flow induced by the stream function ψ_0 captures the main features observed on Saturn (see Figure 7), namely a relative vorticity that is negative and whose longitude-averaged values decrease as we approach the core of the vortex at the North Pole (see the data in [3, 9]).

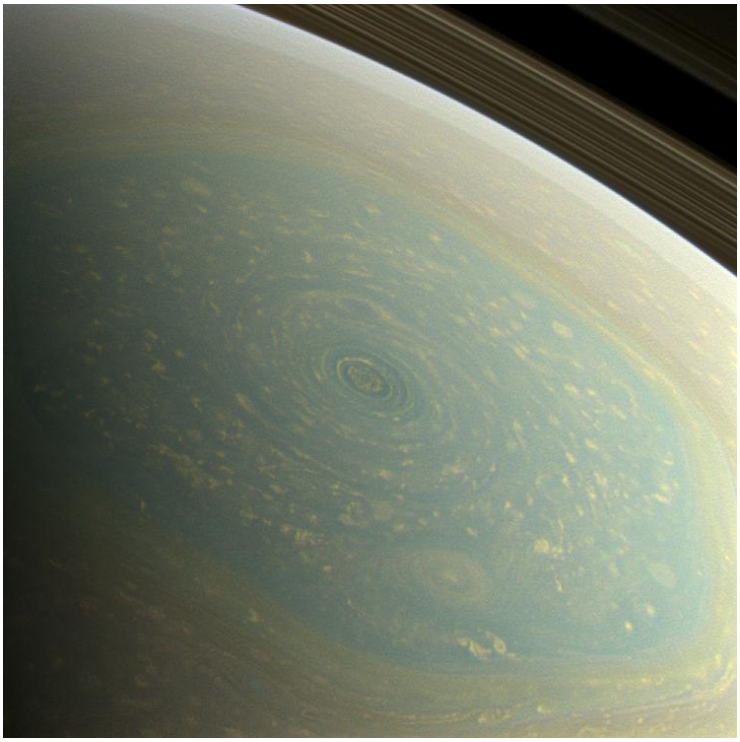

FIGURE 7. The eye of the stationary vortex at Saturn's North Pole (with a surrounding hexagonal jet stream), captured in 2017 by NASA's Cassini spacecraft, is more than 2000 km wide and features prograde wind speeds of 200 $\mathrm{m\,s^{-1}}$ on its outer edge at 88°N (decreasing within the eye to zero at the pole) [Image credit: NASA/JPL-CalTech/Space Science Institute].

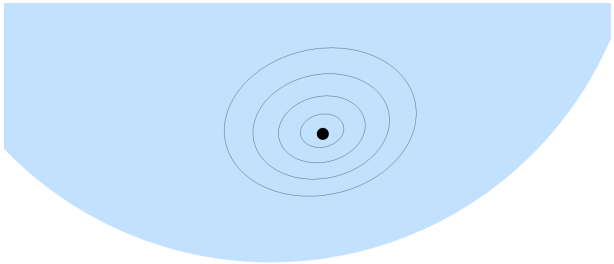

FIGURE 8. Depiction of the streamline pattern (40) inside the polar vortex at the South Pole (the black dot). The velocity and vorticity fields are smooth inside the polar vortex region.

5. **Flow visualization.** The explicit formula for the stream function, (21), offers a wide range of possibilities for the leading-order flow pattern. Other than the two free parameters, the choice of the complex analytic function $f(\zeta)$ allows infinitely-many degrees of freedom. A necessary condition for the estimate (24) to hold is $a < 0$ and $b < 0$ with $ab > 0$. We make the choice $f(\zeta) = \zeta$ with the constants

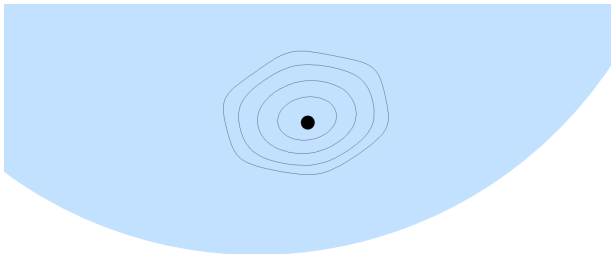

FIGURE 9. Depiction of the streamline pattern inside the polar vortex at the South Pole (the black dot) for the choice (41) with $A = 1$ and $B^6 = .001$. The velocity and vorticity fields are smooth inside the polar vortex region.

$a = -2$ and $b = -1$. (This choice satisfies (33) for Saturn.) The stream function on the stationary sphere, corresponding to this choice, is

$$\psi_0(\zeta, \bar{\zeta}) = 2 \ln \left(\frac{1 - |\zeta|^2}{1 + |\zeta|^2} \right). \tag{40}$$

In the polar vortex region $0 \le |\zeta| \le \delta \ll 1$, this stream function is $O(\delta^2)$ and free from any singularities. The streamlines are circles centered at the South Pole $\zeta = 0$, as shown in Figure 8. The estimate (24) then guarantees that a similar solution ψ exists on the rotating sphere, and quantifies its deviation from (40).

We can also make more complicated choices of f, such as $f(\zeta) = A\zeta(\zeta^6/7 - B^6)$ where A and B are real parameters. In this case the corresponding stream function on the stationary sphere is

$$\psi_0(\zeta, \bar{\zeta}) = -2 \ln \left(\frac{A|\zeta^6 - B^6|(|\zeta|^2 + 1)}{1 - A^2|\zeta|^2|\zeta^6/7 - B^6|^2} \right). \tag{41}$$

Provided $|B| > \delta$, this stream function is free of singularities in $|\zeta| \le \delta$. The streamline pattern, shown in Figure 9, is similar to Figure 8 but is no longer perfectly rotationally symmetric.

6. **Discussion.** Polar vortices are prominent dynamical features of the atmospheric flow on planets in our solar system. Typically, in these spherical cap regions the horizontal velocity field changes rapidly with latitude and thus the vorticity highly concentrates. Field data also reveals a coherent vortex structure near the core. This motivates the study of steady vortex-dominated background states that are characterized by regions of concentrated vorticity. A nonlinear setting is adequate to cope with the strong variations of the relative vorticity near the core of the polar vortex. Moreover, since polar vortices are large-scale rotations of the polar atmosphere near a planet's poles, it is advantageous to retain the spherical geometry.

Starting from the Euler equation expressed in a rotating frame in spherical coordinates, coupled with the equation of mass conservation, we developed a thin-layer (i.e. shallow water) asymptotic approximation. Taking advantage of the fact that the magnitude of the vertical velocity through the layer is much smaller than the horizontal components along the layer, we derived a nonlinear vorticity equation, (1), that models the leading order dynamics of the stream function of a two-dimensional, stratified, steady flow in a polar vortex. In the investigation of this leading-order model one can take advantage of the fact that the effects of rotation are considerably

reduced near the core of the polar vortex. Thus, for polar vortex regions of suitable scales, explicit Stuart-type vortices that model inviscid flow on the surface of a fixed sphere are good approximations for the solutions of the vorticity equation (1). This approach permits us to produce streamline patterns for nonlinear vorticities. The relevant family of explicit solutions presents infinitely-many degrees of freedom in the form of two real parameters and the free choice of a complex analytic function. In particular, we show that we can accommodate solutions that capture the essential features of the atmospheric flow on Saturn's polar vortices: the sign as well as the monotonicity of the relative vorticity within the polar vortex. Moreover, the relevant explicit formula for the stream function, (21), is arguably simpler than the formulas that would emerge by means of spherical harmonics if one were to work within the confines of linear theory.

REFERENCES

[1] A. C. B. Aguiar, P. L. Read, R. D. Wordsworth, T. Salter, R. H. Brown and Y. H. Yamazaki, A laboratory model of of Saturn's North Polar Hexagon, *Icarus*, **206** (2010), 755–763.

[2] K. H. Baines, F. M. Flasar, N. Krupp and T. Stallard, *Saturn in the 21st Century*, Cambridge University Press, 2018.

[3] K. H. Baines, L. A. Sromovsky, P. M. Fry, T. W. Momary, R. H. Brown, B. J. Buratti, R. N. Clark, P. D. Nicholson and C. Sotin, The eye of Saturn's North Polar Vortex: unexpected cloud structures observed at high spatial resolution by Cassini/VIMS, *Geophys. Res. Lett.*, **45** (2018), 5867–5875.

[4] R. Brown, J. P. Lebreton and J. Waite, *Titan from Cassini-Huygens*, Springer, 2014.

[5] A. Constantin and R. S. Johnson, Large gyres as a shallow-water asymptotic solution of Euler's equation in spherical coordinates, *Proc. Roy. Soc. A*, **473** (2017), 20170063.

[6] A. Constantin and V. S. Krishnamurthy, Stuart-type vortices on a rotating sphere, *J. Fluid Mech.*, **865** (2019), 1072–1084.

[7] D. G. Crowdy, General solutions to the 2D Liouville equation, *Intl J. Engng. Sci.*, **35** (1997), 141–149.

[8] D. G. Crowdy, Stuart vortices on a sphere, *J. Fluid Mech.*, **398** (2004), 381–402.

[9] M. K. Dougherty, L. W. Esposito and S. M. Krimigis, *Saturn from Cassini-Huygens*, Springer, 2009.

[10] P. L. Duren, *Theory of H^p spaces*, Academic Press, New York-London, 1970.

[11] N. P. Fofonoff, Steady flow in a frictionless homogeneous ocean, *J. Marine Res.*, **13** (1954), 254–262.

[12] A. E. Gill, *Atmosphere-ocean dynamics*, Academic Press, 1982.

[13] B. Haurwitz, The motion of atmospheric disturbances on a spherical Earth, *J. Marine Res.*, **3** (1940), 254–267.

[14] P. Henrici, *Applied and computational complex analysis. Vol. 3*, John Wiley & Sons, Inc., New York, 1986.

[15] M. S. Longuet-Higgins, Planetary waves on a rotating sphere II, *Proc. R. Soc. A*, **284** (1964), 40–68.

[16] D. M. Mitchell, L. Montabone, S. Thomson and P. L. Read, Polar vortices on Earth and Mars: A comparative study of the climatology and variability from reanalyses, *Quart. J. Roy. Meteorol. Soc.*, **141** (2015), 550–562.

[17] K. Miyazaki and T. Iwasaki, On the analysis of mean downward velocities around the Antarctic Polar Vortex, *J. Atmos. Sci.*, **65** (2008), 3989–4003.

[18] R. Narasimhan, *Analysis on real and complex manifolds*, North-Holland Publishing Co., Amsterdam, 1985.

[19] M. E. O'Neill, K. A. Emanuel and G. R. Flierl, Weak jets and strong cyclones: shallow-water modeling of giant planet polar caps, *J. Atmos. Sci.*, **73** (2016), 1841–1855.

[20] G. Polya and G. Latta, *Complex variables*, John Wiley & Sons, Inc., New York-London-Sydney, 1974.

[21] A. C. Ponce, *Elliptic PDEs, measures and capacities. From the Poisson equations to nonlinear Thomas-Fermi problems*, EMS Tracts in Mathematics, 23, European Math. Soc., Zürich, 2014.

[22] R. K. Scott and D. G. Dritschel, Downward wave propagation on the polar vortex, *J. Atmos. Sci.*, **62** (2005), 3382–3395.
[23] J. T. Stuart, On finite amplitude oscillations in laminar mixing layers, *J. Fluid Mech.*, **29** (1967), 417–440.
[24] G. K. Vallis, *Atmosphere and ocean fluid dynamics*, Cambridge University Press, Cambridge, 2006.
[25] W. T. M. Verkley, The construction of barotropic modons on a sphere, *J. Atmos. Sci.*, **41** (1984), 2492–2505.
[26] T. von Larcher and P. D. Williams, *Modeling atmospheric and oceanic flows*, Amer. Geophys. Union, 2015.
[27] P. Wu and W. T. M. Verkley, Nonlinear structures with multivalued (q, ψ) relationships—exact solutions of the barotropic vorticity equation on a sphere, *Geophys. Astrophys. Fluid Dyn.*, **69** (1993), 77–94.

Received xxxx 20xx; revised xxxx 20xx.

E-mail address: adrian.constantin@univie.ac.at